batteries

MDPI

Article

Application of TiS_2 as an Active Material for Aqueous Calcium-Ion Batteries: Electrochemical Calcium Intercalation into TiS_2 from Aqueous Solutions

Sujin Seong [1], Hajin Lee [2,†], Sangyup Lee [1,†], Paul Maldonado Nogales [1], Changhee Lee [3], Yangsoo Kim [4] and Soon-Ki Jeong [1,5,*]

[1] Department of Energy Engineering, Soonchunhyang University, Soonchunhyang-ro 22-gil, Sinchang-myeon, Asan-si 31538, Chungcheongnam-do, Republic of Korea; 20237060@sch.ac.kr (S.S.); 20237450@sch.ac.kr (S.L.); maldonado@sch.ac.kr (P.M.N.)
[2] ENplus, Free Trade-gil 167 in Baeksan-myeon, Gimje-si 54325, Jeollabuk-do, Republic of Korea; hajin9124@en3.co.kr
[3] Graduate School of Engineering, Kyoto University, Nishikyo-ku, Kyoto 615-8510, Japan; lee.changhee@elech.kuic.kyoto-u.ac.jp
[4] Korea Basic Science Institute, Jeonju Center, Jeonju-si 54907, Jeollabuk-do, Republic of Korea; kimyangsoo@kbsi.re.kr
[5] Advanced Energy Research Center, Soonchunhyang University, Soonchunhyang-ro 22-gil, Sinchang-myeon, Asan-si 31538, Chungcheongnam-do, Republic of Korea
* Correspondence: hamin611@sch.ac.kr; Tel.: +82-41-530-1313
† These authors contributed equally to this work.

Abstract: This study explores the potential of titanium disulfide (TiS_2) as an active material for aqueous calcium-ion batteries (CIBs). We investigate the electrochemical redox reactions of calcium ions within TiS_2 and assess its suitability for use in aqueous CIBs. Additionally, we examine the impact of varying electrolyte concentrations, ranging from 1.0 to 8.0 mol dm^{-3}, on TiS_2 electrode reactions. Our findings reveal that TiS_2 exhibits distinct charge–discharge behaviors in various aqueous calcium-ion electrolytes. Notably, at higher electrolyte concentrations, TiS_2 effectively suppresses the hydrogen generation reaction caused by water decomposition. In situ X-ray diffraction analysis confirms the intercalation of Ca^{2+} ions between the TiS_2 layers during charging, which is a groundbreaking discovery, signifying TiS_2's applicability in aqueous CIBs. X-ray photoelectron spectroscopy analysis further supports the formation of a solid electrolyte interphase (SEI) on the TiS_2 electrode surface, contributing to the suppression of electrolyte decomposition reactions. Furthermore, we investigate the influence of anions in the electrolyte on charge–discharge behavior. Our findings suggest that the choice of anion coordinated with Ca^{2+} ions affects the SEI formation and cycling performance. Understanding the role of anions in SEI formation is crucial for optimizing aqueous CIBs. In conclusion, this research underscores TiS_2's potential as an active material for aqueous calcium-ion batteries and emphasizes the importance of the electrolyte composition in influencing SEI formation and battery performance, contributing to sustainable and efficient energy storage technologies.

Keywords: aqueous calcium battery; titanium disulfide; electrochemical potential window; electrolyte concentration; solid electrolyte interphase; anion

Citation: Seong, S.; Lee, H.; Lee, S.; Nogales, P.M.; Lee, C.; Kim, Y.; Jeong, S.-K. Application of TiS_2 as an Active Material for Aqueous Calcium-Ion Batteries: Electrochemical Calcium Intercalation into TiS_2 from Aqueous Solutions. *Batteries* **2023**, *9*, 500. https://doi.org/10.3390/batteries9100500

Academic Editors: Fernando A. Soto and Xueping Qin

Received: 13 September 2023
Revised: 26 September 2023
Accepted: 29 September 2023
Published: 1 October 2023

1. Introduction

Research into calcium-ion batteries (CIBs), which utilize the redox reaction of calcium ions as an electrode process in secondary batteries, has gained significant momentum recently [1–4]. These batteries offer a promising alternative that could complement and diversify the energy storage landscape [5–9]. Calcium, being relatively abundant and cost-effective compared to certain other metals used in battery technologies, holds the potential to contribute to more sustainable and cost-efficient battery production. This

abundance could play a crucial role in stabilizing renewable energy sources like solar and wind, thereby enhancing grid reliability. Moreover, by reducing our reliance on materials with a high environmental impact, such as cobalt and lithium, CIBs have the potential to foster more sustainable energy storage technologies.

CIBs are categorized into two primary groups determined by the nature of the electrolyte utilized: non-aqueous types [5], which employ organic materials similar to those found in commercially available lithium-ion batteries, and aqueous types [7], which use water-based materials. The choice between organic and aqueous electrolytes depends on specific battery application requirements, encompassing energy density, power output, safety considerations, and the environmental impact. Organic electrolytes offer higher energy densities and broader voltage windows [2,5,8], while aqueous electrolytes provide enhanced safety and environmental benefits [2,3,5,7,10]. Each type of electrolyte has its advantages and disadvantages, and the selection depends on the trade-offs acceptable for the particular battery system being developed. While most existing studies predominantly focus on the former category, there is a limited number of reports on the latter type.

The investigation of electrode materials for aqueous CIBs is an emerging research area. Our focus in this study was directed towards titanium disulfide (TiS_2). TiS_2 stands as a thoroughly investigated electrode material, recognized for its involvement in an intercalation–deintercalation reaction [10–26]. This reaction involves the intercalation and deintercalation of metal ions within its layered crystal structure during charge and discharge cycles, enabling energy storage and release. Notably, this phenomenon is true for non-aqueous CIBs as well [24,25]. Within non-aqueous solutions, the electrochemical intercalation and deintercalation of calcium ions into TiS_2 have been observed. However, it is surprising that TiS_2 has not been investigated as an electrode material for aqueous calcium CIBs. This gap in the research serves as the primary motivation behind the present study.

The purpose of this study is to understand the electrochemical redox reaction of calcium ions in TiS_2 and, through this, to assess the applicability of TiS_2 as an active material for aqueous CIBs. Additionally, the authors aim to understand the effect of the electrolyte on the TiS_2 electrode reaction.

2. Materials and Methods

2.1. Preparation of Electrode and Electrolytes

TiS_2 powder (Sigma-Aldrich, 99.9%, St. Louis, MO, USA) served as the working electrode. A slurry was prepared by mixing TiS_2, carbon black (super P) (Alfa Aesar, 99+%, Harverhill, MA, USA), graphite powder (SNO-15), and polyvinylidene fluoride (Sigma-Aldrich, average Mw ~534,000 by GPC, powder, St. Louis, MO, USA) in an 80:9:2:9 weight ratio using N-Methyl-2-pyrrolidone (NMP) (JUNSEI, 99+%, Tokyo, Japan) as the solvent. The resulting slurry was coated onto a current collector and dried for 12 h at 80 °C under a vacuum. For the $Ca(NO_3)_2^-$ and $CaCl_2$-based electrolytes, carbon cloth (Fuelcellearth, Woburn, MA, USA) and Ti foil (Nilaco, 99.5%, Tokyo, Japan) were utilized as current collectors, respectively. When using the carbon cloth current collector, the loaded mass of TiS_2 was 1.81 ± 0.4 mg cm^{-2}, whereas with the Ti foil current collector, it was 2.30 ± 0.5 mg cm^{-2}. Activated carbon powder (Sigma-Aldrich, −100 mesh particle size, St. Louis, MO, USA) was employed as the counter electrode. To prepare the slurry, activated carbon and polyvinylidene fluoride were mixed in a 9:1 weight ratio using NMP as the solvent. This slurry was applied to the same current collector used for the working electrode and dried for 12 h at 80 °C under a vacuum. When using the carbon cloth current collector, the loaded mass of activated carbon was 8.43 ± 1.4 mg cm^{-2}, whereas with the Ti foil current collector, it was 3.28 ± 2.6 mg cm^{-2}.

Electrolytes were formulated by dissolving $Ca(NO_3)_2{\cdot}4H_2O$ (Alfa Aesar, 99–103%, Harverhill, MA, USA) and $CaCl_2{\cdot}2H_2O$ (Alfa Aesar, 99.0–105.0%, Harverhill, MA, USA) in pure water (Burdick & Jackson, HPLC grade, Muskegon, MI, USA), respectively. Different electrolyte concentrations (1.0, 4.0, 7.0, and 8.0 mol dm^{-3} (M)) were employed to investigate variations in the electrochemical potential window and electrochemical performance based

on the concentration. The maximum concentration of 8.0 M was chosen considering the solubility of calcium salts.

2.2. Electrochemical Measurements

All electrochemical tests were performed using a custom-designed laboratory three-electrode cell within a battery test system (Wonatech, WBCS 3000, Seoul, Republic of Korea). The prepared TiS_2 electrode served as the working electrode, while the activated carbon electrode was employed as the counter electrode. A saturated calomel electrode (SCE) (Qrins, RE-2BP, 3.3 M potassium chloride, Seoul, Republic of Korea) was used as the reference electrode. Charge–discharge testing encompassed 5 cycles at a 0.1 C-rate (C), spanning a potential range from −1.0 to 0.76 V (vs. SCE). These tests were carried out using $Ca(NO_3)_2$ and $CaCl_2$ electrolytes at varying concentrations.

2.3. Structure and Surface Analysis

Modifications in the structure and surface composition of the TiS_2 electrode before and after charging and discharging were confirmed through X-ray diffraction (XRD) (Rigaku, Miniflex 600, Tokyo, Japan) and X-ray photoelectron spectroscopy (XPS) (Kratos Analytical, Axis-Nova, Manchester, UK) analyses. In situ XRD analyses revealed alterations in interlayer spacing during the charging and discharging process of the TiS_2 electrode within the 2θ range of 10–80°. For in situ XRD analysis, a self-fabricated laboratory cell (illustrated in Figure 1) was employed. The working electrode was prepared by applying the slurry, as described in Section 2.1, onto a polyimide film (DuPont, 25 µm thick Kapton® 100HN film, Wilmington, DE, USA), and then affixing the prepared film to a Ti plate (Nilaco, 0.15T, Tokyo, Japan), which served as the current collector. To mitigate the influence of activated carbon on X-ray diffraction, a Pt mesh (WizMAC, net type, Daejeon, Republic of Korea) was employed as the counter electrode, with SCE serving as the reference electrode. The electrolyte used was 8.0 M $Ca(NO_3)_2$, and charge/discharge test conditions matched those previously mentioned. Moreover, XPS was utilized to analyze the binding energy of calcium ions on the electrode surface after charging and discharging. Depth analysis was performed at 20 and 40 s after etching the surface with an argon ion laser.

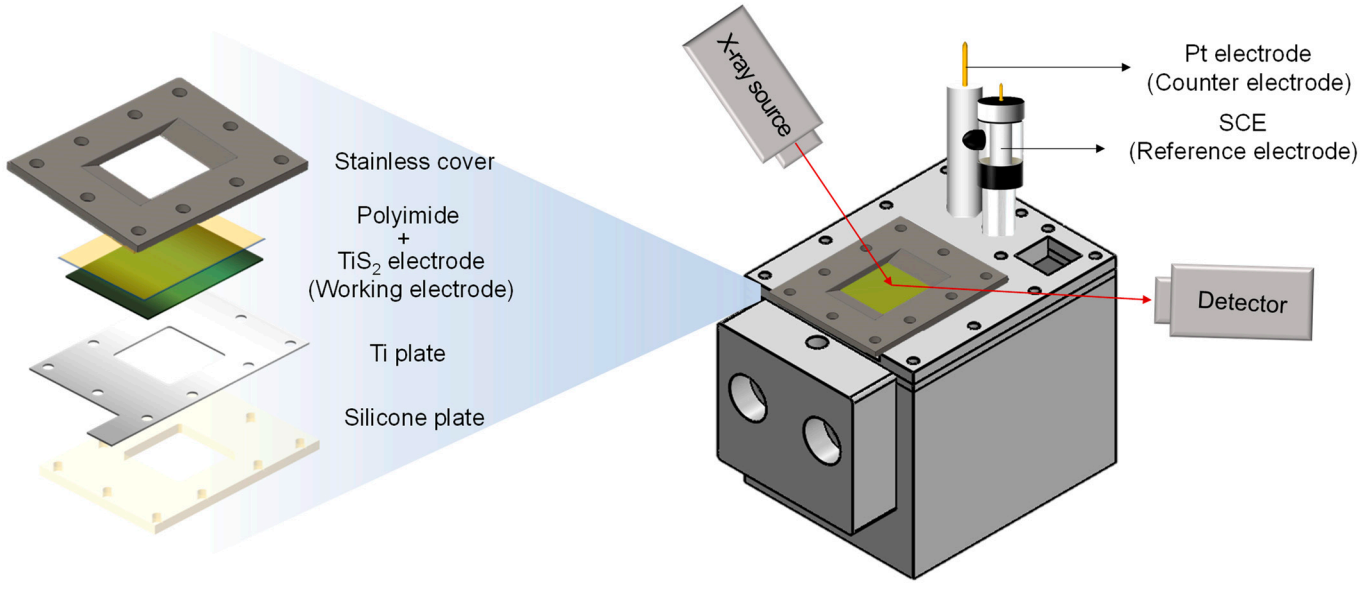

Figure 1. Schematic illustration of the self-fabricated three-electrode cell configuration used for in situ XRD measurements.

3. Results and Discussion

3.1. Dependence of Charge–Discharge Behavior on Electrolyte Concentration

Figure 2 depicts the electrochemical potential behavior of TiS_2 in aqueous solutions based on $Ca(NO_3)_2$ with varying concentrations. In both the 1.0 and 4.0 M electrolyte solutions, the TiS_2 electrode exhibited a nearly identical potential behavior, maintaining a steady level around 0.5 V, as presented in Figure 2a,b. It was visually confirmed that gas emerged from the electrode surface during this process. This gas was identified as hydrogen, resulting from the reductive decomposition of water molecules within the electrolyte solution. In other words, this means that TiS_2 does not function as an active material for aqueous CIBs due to the fact that the water decomposition reaction takes place prior (at a more positive potential) to the intercalation of calcium ions between the layers of TiS_2. In contrast, with the 7.0 and 8.0 M electrolyte solutions, the electrode potential dropped to −1.0 V during the reduction of Ca^{2+} ions, resulting in the verified charge capacity presented in Figure 2c,d. Subsequently, the discharge capacity from the oxidation reaction was also confirmed. This demonstrates the effectiveness of TiS_2 as an active material for aqueous CIBs, effectively suppressing the hydrogen generation reaction caused by water decomposition.

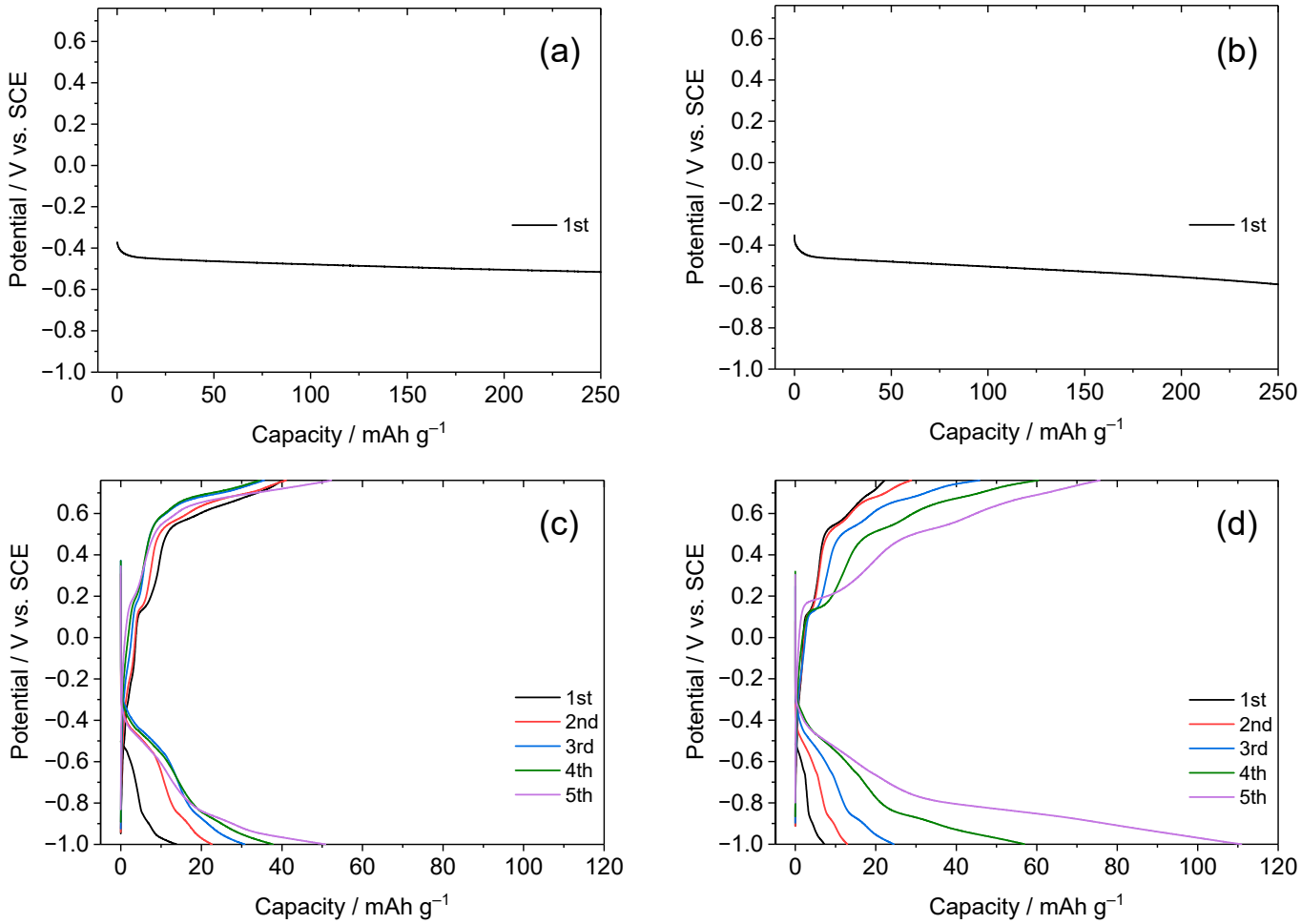

Figure 2. Charge and discharge curves of TiS_2 electrode in aqueous solutions with varied $Ca(NO_3)_2$ concentrations: (**a**) 1.0, (**b**) 4.0, (**c**) 7.0, and (**d**) 8.0 M. The measurements were conducted at a 0.1 C-rate.

The suppression of the hydrogen generation reaction can be attributed to the decomposition of anions preceding water decomposition, resulting in a film forming on the electrode surface. This phenomenon is closely tied to changes in the solvation structure of Ca^{2+} ions at higher concentrations. An increased concentration leads to higher counts of both Ca^{2+}

and NO_3^- ions in the electrolyte. Previous studies have shown that not only water, but also NO_3^- ions coordinate with Ca^{2+} ions under these conditions [27–34]. Consequently, the number of water molecules coordinating with each Ca^{2+} ion decreases. This results in the generation of numerous contact ion pairs in the electrolyte solution, leading to ion aggregation [35–39]. In this process, NO_3^- ions transfer electrons to Ca^{2+} ions, resulting in a reduction of the energy level of the low unoccupied molecular orbital (LUMO) of NO_3^- ions [18,27–29,31,39]. Consequently, it is hypothesized that NO_3^- ions undergo preferential reduction (at more positive potentials) prior to water decomposition. This preference leads to the generation of a film derived from NO_3^- on the electrode surface. This can be comprehended as a phenomenon closely resembling the anion-derived solid electrolyte interphase (SEI) formed on the surface of a negative electrode when an aqueous solution with a high concentration of Li^+ ions is employed as the electrolyte [39–42]. Similarly, a NO_3^--derived SEI forms on the surface of TiS_2 electrode within an aqueous solution containing a high concentration of Ca^{2+} ions, suppressing electrolyte decomposition reactions such as hydrogen generation and promoting intercalation and deintercalation reactions of Ca^{2+} ions.

Another notable feature in Figure 2c is the considerably larger discharge capacity compared to the charge capacity. Moreover, as the cycling progressed, the charge capacity gradually increased, narrowing the gap between the charging and discharging capacities. This suggests that, during discharge, the deintercalation of Ca^{2+} ions occurred alongside the oxidation reaction of the electrolyte. The effectiveness of the NO_3^--derived film as an SEI improved during cycling. A similar trend is also evident in Figure 2d. However, a slightly distinct observation is that the charge capacity exhibited a more pronounced increase than that in Figure 2c, implying more effective SEI formation in higher concentrations. This supports the notion that the SEI formation is driven by the reduction of NO_3^- ions with lower LUMO energy levels due to their coordination with Ca^{2+} ions. This phenomenon is attributed to the greater presence of NO_3^- ions with lower LUMO energy levels due to coordination with Ca^{2+} ions in the 8.0 M aqueous solution compared to those in the 7.0 M solution.

3.2. In Situ Structural Analysis of TiS_2 during Charging and Discharging

The charge and discharge behaviors of the TiS_2 electrode were significantly influenced by the electrolyte concentration, as discussed previously. To confirm the intercalation and deintercalation of Ca^{2+} ions into and from TiS_2 at higher concentrations, we employed in situ XRD. This technique allowed us to examine the associated structural modifications in detail. Figure 3 presents the XRD patterns of TiS_2 in an 8.0 M $Ca(NO_3)_2$ solution collected during the charge and discharge processes using the three-electrode cell shown in Figure 1. A strong (002) peak of the pristine electrode was observed at 31.4° in 2θ. This peak gradually shifted to a lower angle during the charging process, reaching 31.1° after being charged to −1.0 V. This shift corresponds to an expansion of the interlayer spacing due to the intercalation of Ca^{2+} ions between the TiS_2 layers. To the best of our knowledge, this is the first confirmation of the electrochemical intercalation of calcium ions between the TiS_2 layers in an aqueous electrolyte solution. While previous reports have described the insertion of calcium ions using an organic electrolyte with a wide potential window [24,25], there has been no prior report of calcium ion insertion using an aqueous solution with a much narrower potential window compared to that of the organic electrolyte. In other words, this suggests that TiS_2 can serve as an active material in aqueous CIBs.

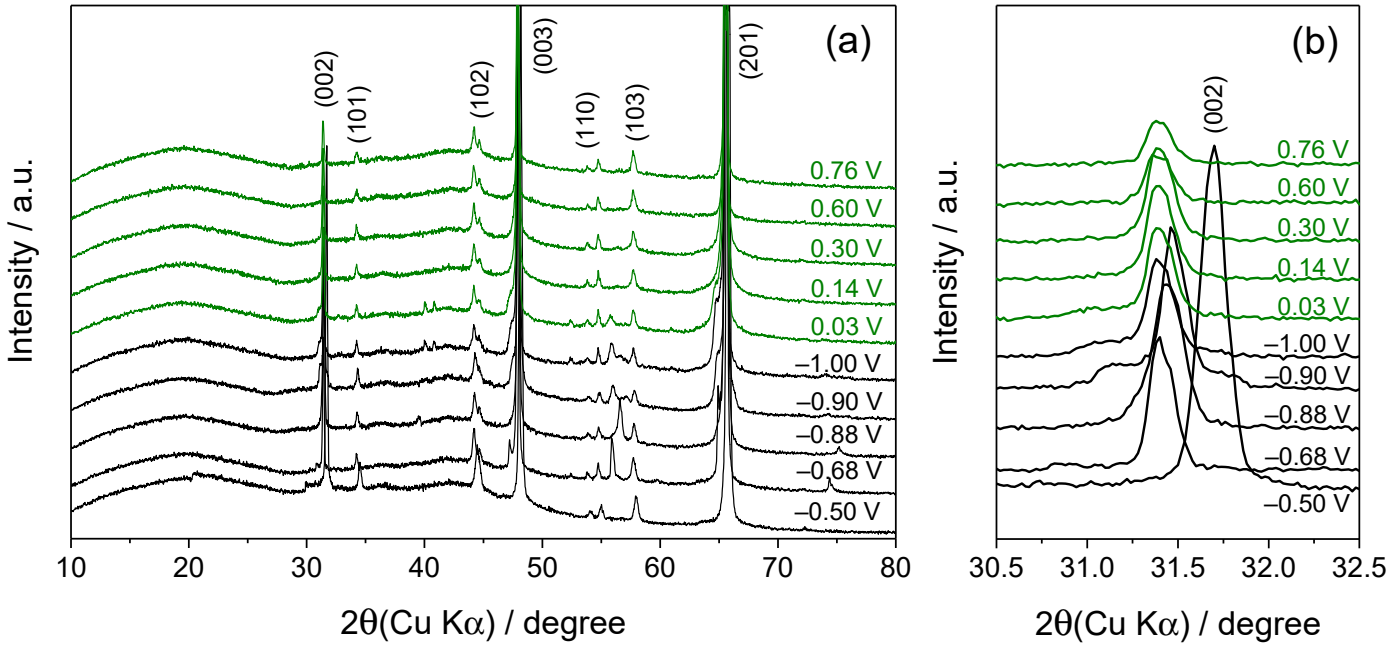

Figure 3. (**a**) In situ XRD patterns during the charge–discharge test of TiS_2 electrode in an 8.0 M $Ca(NO_3)_2$ dissolved aqueous electrolyte at a voltage range between −1.0 and 0.76 V. (**b**) shows the enlarged view of the (002) peak regions in Figure 3a.

On the other hand, the (002) peak, which shifted during charging, did not revert to its original position during discharge. Instead, it remained in the shifted position after charging was completed. This phenomenon likely results from the partial retention of Ca^{2+} ions within the TiS_2 structure, as further explained in the XPS analysis results. These intercalated Ca^{2+} ions do not completely deintercalate during discharge, continuing to occupy the interlayer spaces. Tchitchekova et al. conducted a study on the diffusion behavior of Ca^{2+} ions when the interlayer spacing of TiS_2 expanded by 10% and 15% based on DFT calculations [24]. Their findings indicated a reduced activation barrier to Ca^{2+} ion diffusion due to the expanded interlayer spacing. Therefore, it is reasonable to assume that the observed expansion of the interlayer gap in Figure 3, along with the improvements in the SEI described in the previous section, facilitated the diffusion of Ca^{2+} ions, leading to an increase in capacity during cycling.

Another noteworthy observation in Figure 3 is the broadening of the (002) peak after a single charge–discharge cycle. This suggests a decrease in the crystallinity of the TiS_2 active material. Although the exact cause remains unclear, one plausible explanation is the nonuniform diffusion of inserted ions [43]. When metal ions intercalate between TiS_2 layers, they induce phase separation in TiS_2. The high-resolution transmission electron microscopy results acquired by the Li group revealed that TiS_2 undergoes a stepwise phase transformation during the intercalation of K^+ ions, resulting in the uneven diffusion of these ions [22]. This stepwise phase transformation is not limited to K^+ ions; it also occurs during the intercalation of Na^+ ions [44]. In essence, it is presumed that the crystallinity deteriorated even after discharge due to the incomplete desorption of all the unevenly intercalated Ca^{2+} ions.

3.3. XPS Analysis of TiS_2 Electrode before and after Discharging

To investigate the intercalation–deintercalation behavior of Ca^{2+} ions and the formation of an SEI, we conducted XPS analysis on TiS_2 electrodes in both their charged and discharged states, and the results are depicted in Figure 4. After charging (Figure 4b), two distinct peaks emerged at approximately 348.4 and 351.9 eV, corresponding to the binding energies of Ca $2p_{3/2}$ and Ca $2p_{1/2}$, respectively [45]. The approximate 3.5 eV difference between these peaks is attributed to spin–orbit splitting. These peaks indicate

the formation of calcium compounds on the electrode surface as a result of anion reduction coordinated with Ca^{2+} ions. Even after etching for 40 s, these peaks persisted, suggesting the presence of Ca atoms not only on the electrode surface, but also within the TiS_2 layers. This implies the intercalation of Ca^{2+} ions between TiS_2 layers, indicating that the calcium compound generated on the electrode surface functions as the SEI. This SEI may either dissolve or undergo changes in its properties when exposed to free water molecules that are not coordinated with Ca^{2+} ions [30]. However, in high-concentration electrolyte solutions, where free water molecules are scarce, the SEI is be lieved to function effectively.

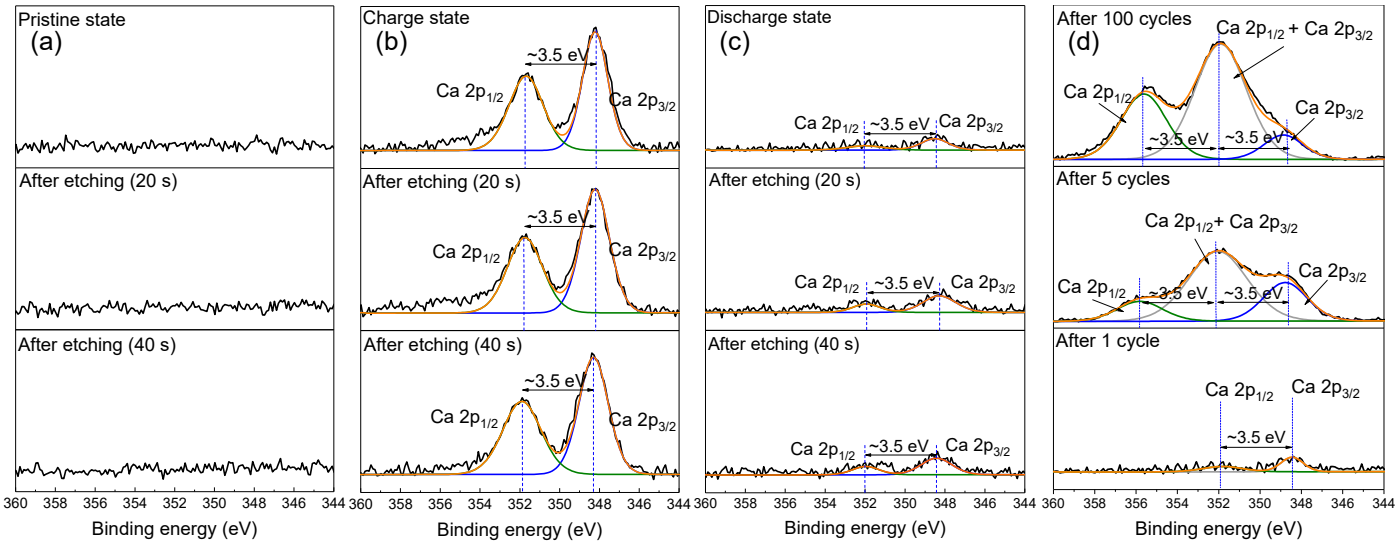

Figure 4. (**a**–**d**) The Ca 2p region of XPS spectra of the TiS_2 electrode, including both unetched and etched samples at 20 and 40 s. (**a**) Pristine, (**b**) charge, and (**c**) discharge states. (**d**) Ca 2p region of the XPS spectra in the pristine state after 1, 5, and 100 cycles of the TiS_2 electrode. Black lines: experimental data; orange lines: fitted curves; green, gray, and blue lines: deconvoluted bands.

On the other hand, in the discharged state (Figure 4c), the peak intensity decreased more compared to the charged state, but did not vanish entirely. Two peaks were observed at the same positions as in the charged state, indicating that some Ca^{2+} ions remained intercalated between the TiS_2 layers. These remaining Ca^{2+} ions may have been directly responsible for both maintaining the expanded interlayer gap of TiS_2 and lowering the crystallinity of TiS_2 even after the discharge previously shown in Figure 3.

To further investigate the evolution of the SEI on the surface of the TiS_2 electrode as cycling progressed, the Ca 2p binding energy on the TiS_2 electrode was examined after 1, 5, and 100 cycles, as shown in Figure 4d. As cycling continued, the peak area increased, indicating an increase in calcium compounds due to electrolyte decomposition during the repair of the damaged SEI caused by the expansion and contraction of the active material (TiS_2) over 100 charge–discharge cycles. Furthermore, with ongoing cycling, the peak area around ~348.4 eV decreased, while the area around ~351.9 eV increased, and a new peak emerged at ~355.4 eV. This change in peak area and the appearance of a new peak can be attributed to a peak shift of Ca 2p by approximately ~3.5 eV in some of the initially formed calcium compounds. Such shifts usually occur due to changes in the chemical environment of the calcium atom [46,47]. While it remains unclear which specific factors induce these shifts and why only some Ca 2p peaks are affected, identifying these factors will be crucial for future research in this study.

3.4. Anion Dependence of Charge–Discharge Behavior

As previously mentioned, we have confirmed the occurrence of electrochemical intercalation–deintercalation reactions involving Ca^{2+} ions in a TiS_2 electrode. This confirmation was achieved using aqueous solutions containing a high concentration of $Ca(NO_3)_2$

as the electrolyte. The enabling factor for this intercalation process lies in the formation of the SEI on the surface of the TiS_2 electrode. Our interpretation is that the reduction of anions plays a crucial role in SEI generation. To further substantiate this interpretation, we prepared an aqueous solution with a high concentration of $CaCl_2$ instead of $Ca(NO_3)_2$ and subsequently investigated the charging and discharging behaviors within this solution. Essentially, we altered the anion coordinated with Ca^{2+} ions from NO_3^- to Cl^- to assess the impact of the anion on the charge and discharge behaviors. The results of this experiment are presented in Figure 5.

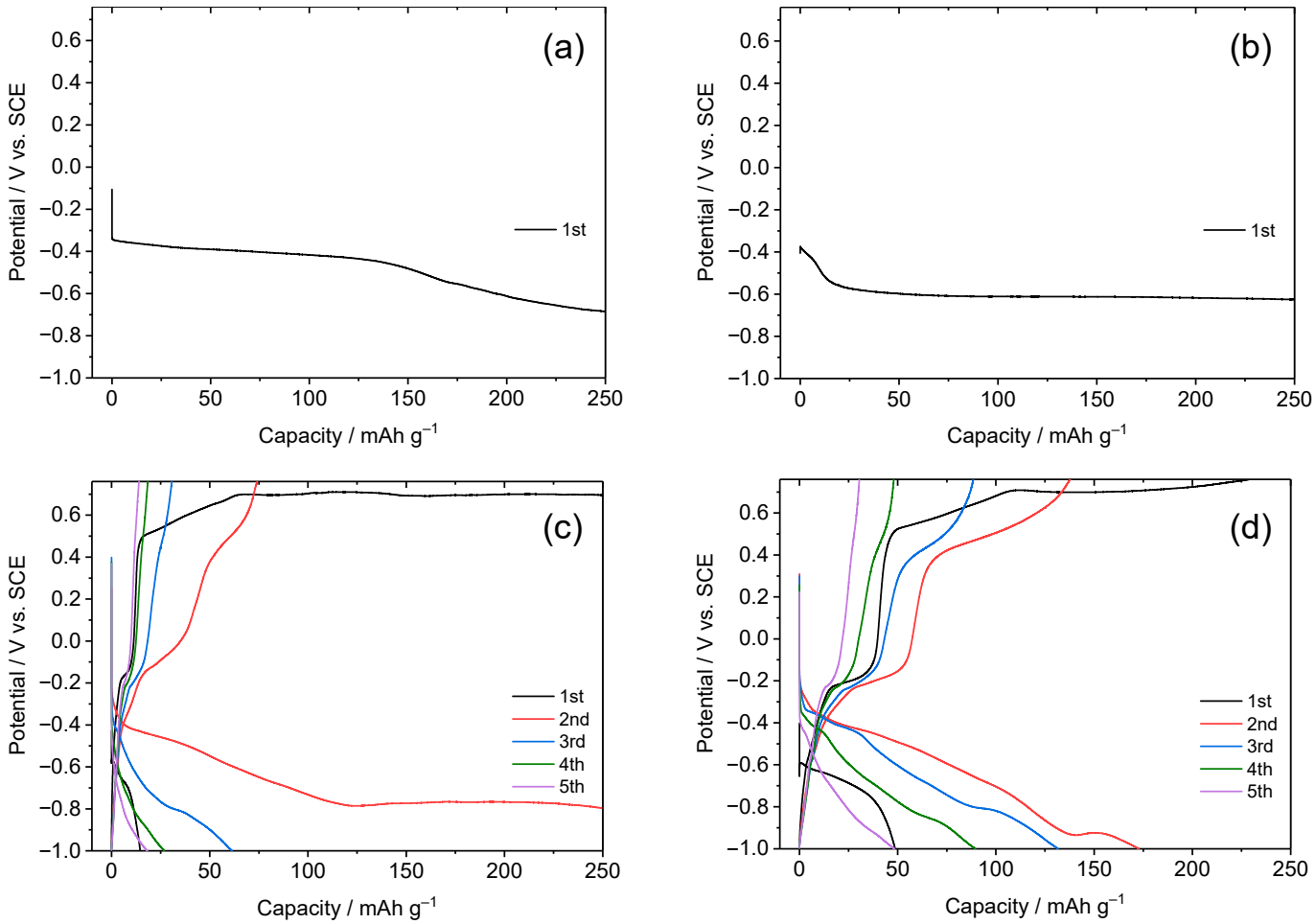

Figure 5. Charge and discharge curves of TiS_2 electrode in aqueous solutions with varied $CaCl_2$ concentrations: (**a**) 1.0, (**b**) 4.0, (**c**) 7.0, and (**d**) 8.0 M. The measurements were conducted at a 0.1 C-rate.

In the $CaCl_2$-based aqueous solution, we observed a charge–discharge behavior similar to what was obtained in the $Ca(NO_3)_2$-based aqueous solution (as confirmed in Figure 2). Notably, the charging and discharging of the TiS_2 electrode were not possible at 1.0 and 4.0 M concentrations, but they became feasible at 7.0 and 8.0 M. Previous research has noted that at high concentrations, $CaCl_2$-based aqueous solutions form contact ion pairs similar to those in $Ca(NO_3)_2$-based aqueous solutions [48,49]. Consequently, the coordination of Ca^{2+} ions with water molecules decreases, while Cl^- ions become involved in coordination [48,49]. In high-concentration environments, it can be anticipated that the energy level of the LUMO of Cl^- ions will decrease, resulting in a higher reduction potential. With this information, we can explain the stark differences in charge and discharge behaviors shown in Figure 5 by dividing them into two cases: first, the reduction reaction of water molecules generating hydrogen occurs, preventing charge and discharge (Figure 5a,b);

second, the reduction reaction of Cl^- ions, producing an SEI, takes place first, allowing subsequent charging and discharging (Figure 5c,d). The discharge capacity obtained from the 8.0 M solutions, as depicted in Figures 5d and 2d, is comparable to the capacities of previously reported materials [7,34,50]. There are very few materials known for their ability to store calcium ions for aqueous CIBs. In addition to TiS_2, the following materials have been confirmed for calcium insertion through electrochemical experiments with or without electrolyte solvents: poly[*N*,*N*′-(ethane-1,2-diyl)-1,4,5,8-naphthalenetetracarboxiimide] [7], 5,7,12,14-pentacenetetrone [50], copper hexacyanoferrate [34], MoO_x [51], and a covalent organic framework [52]. Their initial capacities are approximately 160, 125, 80, 60, and 120 mAh g^{-1}, respectively. While each of these materials possesses unique characteristics, there are still challenges to overcome before effectively utilizing them as electrode materials for CIBs.

Notably, the irreversible capacity and cycling behavior exhibited significant deviations from those observed in the $Ca(NO_3)_2$-based aqueous solution. In the initial cycle, the discharge capacity surpassed the charge capacity, suggesting that, in addition to the deintercalation of Ca^{2+} ions during discharge, there were concurrent decomposition reactions involving the electrolyte or SEI formed during charging. Furthermore, as cycling continued, there was a rapid decrease in the discharge capacity. We attribute these differences in the irreversible capacity and cycling behavior to variations in the properties of the SEI formed in each electrolyte solution. In essence, once the SEI forms through electrolyte decomposition, it should ideally restrain further electrolyte decomposition, while allowing the smooth passage of metal ions during subsequent cycles to maintain stability. Consequently, it is evident that discrepancies in charging and discharging behaviors arise due to differences in the SEI's ability to fulfill these essential functions.

4. Conclusions

In this study, we explored the potential of TiS_2 as an active material for aqueous CIBs, focusing on the electrochemical redox reaction of calcium ions. We examined the dependence of charge–discharge behavior on electrolyte concentration, revealing that TiS_2 effectively suppresses hydrogen generation in higher electrolyte concentrations. This suppression is attributed to the formation of an anion-derived SEI on the electrode surface, facilitated by changes in the solvation structure of Ca^{2+} ions at higher concentrations. Additionally, in situ structural analysis using XRD confirmed the intercalation of Ca^{2+} ions into TiS_2 during charging, marking the first confirmation of this electrochemical intercalation in an aqueous electrolyte solution. XPS analysis supported this, indicating Ca atoms within TiS_2 layers and on the electrode surface. Furthermore, our study investigated the influence of anions on charge–discharge behavior by comparing $Ca(NO_3)_2$- and $CaCl_2$-based electrolytes. The results showed that the choice of anion had a significant impact on SEI formation, and consequently, on the charge–discharge behavior. While both electrolytes allowed TiS_2 to function as an active material at higher concentrations, variations in the irreversible capacity and cycling behavior highlighted the importance of SEI properties in dictating the performance of CIBs. In conclusion, our findings demonstrate that TiS_2 holds promise as an active material for aqueous CIBs, providing insights into the crucial role of SEI formation and anion choice in influencing CIB performance. In future studies, it is necessary to investigate the properties (composition, thickness, resistance, electrochemical stability, etc.) of the SEI formed on the TiS_2 electrode surface due to electrolyte decomposition and clarify its direct relationship with cycling stability.

Author Contributions: Conceptualization, S.S., H.L. and S.-K.J.; methodology, H.L., P.M.N. and Y.K.; formal analysis, S.S., H.L., S.L. and C.L.; investigation, S.S. and H.L.; resources, S.S. and H.L.; data curation, S.S. and H.L.; writing—original draft preparation, S.S., H.L. and S.L.; writing—review and editing, S.S., S.L. and S.-K.J.; supervision, S.-K.J.; project administration, S.-K.J.; funding acquisition, S.-K.J. All authors have read and agreed to the published version of the manuscript.

Funding: This research was supported by Basic Science Research Program through the National Research Foundation of Korea (NRF) funded by the Ministry of Education (NRF-2021R1I1A3060329). This work was supported by Korea Institute for Advancement of Technology (KIAT) grant funded by the Korea Government (MOTIE) (1415182582, Automotive Industry Technology Development). This work also received support from the Soonchunhyang University Research Fund.

Data Availability Statement: Not applicable.

Conflicts of Interest: The authors declare no conflict of interest.

References

1. Zaman, W.; Hatzell, K.B. Processing and manufacturing of next generation lithium-based all solid-state batteries. *Curr. Opin. Solid State Mater. Sci.* **2022**, *26*, 101003. [CrossRef]
2. Chen, S.; Jeong, S.R.; Tao, S. Key materials and future perspective for aqueous rechargeable lithium-ion batteries. *Mater. Rep. Energy* **2022**, *2*, 100096. [CrossRef]
3. Shin, J.; Choi, J.W. Opportunities and reality of aqueous rechargeable batteries. *Adv. Energy Mater.* **2020**, *10*, 2001386. [CrossRef]
4. Tran, M.-K.; Mevawalla, A.; Aziz, A.; Panchal, S.; Xie, Y.; Fowler, M. A review of lithium-ion battery thermal runaway modeling and diagnosis approaches. *Processes* **2022**, *10*, 1192. [CrossRef]
5. Ji, B.; He, H.; Yao, W.; Tang, Y. Recent advances and perspectives on calcium-ion storage: Key materials and devices. *Adv. Mater.* **2021**, *33*, 2005501. [CrossRef]
6. Li, X.; Wang, X.; Ma, L.; Huang, W. Solvation structures in aqueous metal-ion batteries. *Adv. Energy Mater.* **2022**, *12*, 2202068. [CrossRef]
7. Gheytani, S.; Liang, Y.; Wu, F.; Jing, Y.; Dong, H.; Rao, K.K.; Chi, X.; Fang, F.; Yao, Y. An aqueous Ca-ion battery. *Adv. Sci.* **2017**, *4*, 1700465. [CrossRef]
8. Lee, C.; Jeong, S.-K. A novel strategy to improve the electrochemical performance of a prussian blue analogue electrode for calcium-ion batteries. *Electrochemistry* **2018**, *86*, 134–137. [CrossRef]
9. Purbarani, M.E.; Hyoung, J.; Hong, S.-T. Crystal-water-free potassium vanadium bronze ($K_{0.5}V_2O_5$) as a cathode material for Ca-ion batteries. *ACS Appl. Energy Mater.* **2021**, *4*, 7487–7491. [CrossRef]
10. Alvarez Ferrero, G.; Åvall, G.; Mazzio, K.A.; Son, Y.; Janßen, K.; Risse, S.; Adelhelm, P. Co-intercalation batteries (CoIBs): Role of TiS_2 as electrode for storing solvated Na ions. *Adv. Energy Mater.* **2022**, *12*, 2202377. [CrossRef]
11. Whittingham, M.S. Electrical energy storage and intercalation chemistry. *Science* **1976**, *192*, 1126–1127. [CrossRef]
12. Whittingham, M.S. Chemistry of intercalation compounds: Metal guests in chalcogenide hosts. *Prog. Solid State Chem.* **1978**, *12*, 41–99. [CrossRef]
13. Wang, H.; Qiu, Z.; Xia, W.; Ming, C.; Han, Y.; Cao, L.; Lu, J.; Zhang, P.; Zhang, S.; Xu, H. Semimetal or semiconductor: The nature of high intrinsic electrical conductivity in TiS_2. *J. Phys. Chem. Lett.* **2019**, *10*, 6996–7001. [CrossRef] [PubMed]
14. Wang, B.; Bates, J.; Hart, F.; Sales, B.; Zuhr, R.; Robertson, J. Characterization of thin-film rechargeable lithium batteries with lithium cobalt oxide cathodes. *J. Electrochem. Soc.* **1996**, *143*, 3203. [CrossRef]
15. Striebel, K.; Deng, C.; Wen, S.; Cairns, E. Electrochemical behavior of $LiMn_2O_4$ and $LiCoO_2$ Thin films produced with pulsed laser deposition. *J. Electrochem. Soc.* **1996**, *143*, 1821. [CrossRef]
16. Prosini, P.P.; Lisi, M.; Zane, D.; Pasquali, M. Determination of the chemical diffusion coefficient of lithium in $LiFePO_4$. *Solid State Ion.* **2002**, *148*, 45–51. [CrossRef]
17. Sun, X.; Bonnick, P.; Nazar, L.F. Layered TiS_2 positive electrode for Mg batteries. *ACS Energy Lett.* **2016**, *1*, 297–301. [CrossRef]
18. Zhang, L.; Hou, X.; Edström, K.; Berg, E.J. Reactivity of TiS_2 anode towards electrolytes in aqueous lithium-ion batteries. *Batter. Supercaps* **2022**, *5*, e202200336. [CrossRef]
19. Sun, W.; Suo, L.; Wang, F.; Eidson, N.; Yang, C.; Han, F.; Ma, Z.; Gao, T.; Zhu, M.; Wang, C. "Water-in-salt" electrolyte enabled $LiMn_2O_4/TiS_2$ lithium-ion batteries. *Electrochem. Commun.* **2017**, *82*, 71–74. [CrossRef]
20. Chung, S.-H.; Luo, L.; Manthiram, A. TiS_2–polysulfide hybrid cathode with high sulfur loading and low electrolyte consumption for lithium–sulfur batteries. *ACS Energy Lett.* **2018**, *3*, 568–573. [CrossRef]
21. Tian, B.; Tang, W.; Leng, K.; Chen, Z.; Tan, S.J.R.; Peng, C.; Ning, G.-H.; Fu, W.; Su, C.; Zheng, G.W. Phase transformations in TiS_2 during K intercalation. *ACS Energy Lett.* **2017**, *2*, 1835–1840. [CrossRef]
22. Wang, L.; Zou, J.; Chen, S.; Zhou, G.; Bai, J.; Gao, P.; Wang, Y.; Yu, X.; Li, J.; Hu, Y.-S. TiS_2 as a high performance potassium ion battery cathode in ether-based electrolyte. *Energy Storage Mater.* **2018**, *12*, 216–222. [CrossRef]
23. Hu, Z.; Tai, Z.; Liu, Q.; Wang, S.W.; Jin, H.; Wang, S.; Lai, W.; Chen, M.; Li, L.; Chen, L. Ultrathin 2D TiS_2 nanosheets for high capacity and long-life sodium ion batteries. *Adv. Energy Mater.* **2019**, *9*, 1803210. [CrossRef]
24. Tchitchekova, D.S.; Ponrouch, A.; Verrelli, R.; Broux, T.; Frontera, C.; Sorrentino, A.; Bardé, F.; Biskup, N.; Arroyo-de Dompablo, M.E.; Palacin, M.R. Electrochemical intercalation of calcium and magnesium in TiS_2: Fundamental studies related to multivalent battery applications. *Chem. Mater.* **2018**, *30*, 847–856. [CrossRef]
25. Lee, C.; Jeong, Y.-T.; Nogales, P.M.; Song, H.-Y.; Kim, Y.; Yin, R.-Z.; Jeong, S.-K. Electrochemical intercalation of Ca^{2+} ions into TiS_2 in organic electrolytes at room temperature. *Electrochem. Commun.* **2019**, *98*, 115–118. [CrossRef]

26. Huang, C.; Liu, Y.; Li, J.; Miao, Z.; Cai, X.; Wu, Z.; Yu, H.; Yan, L.; Zhang, L.; Shu, J. Organic interlayer engineering of TiS_2 for enhanced aqueous Zn ions storage. *J. Mater. Sci. Technol.* **2023**, *140*, 135–141. [CrossRef]
27. Suo, L.; Borodin, O.; Gao, T.; Olguin, M.; Ho, J.; Fan, X.; Luo, C.; Wang, C.; Xu, K. "Water-in-salt" electrolyte enables high-voltage aqueous lithium-ion chemistries. *Science* **2015**, *350*, 938–943. [CrossRef]
28. Yamada, Y.; Usui, K.; Sodeyama, K.; Ko, S.; Tateyama, Y.; Yamada, A. Hydrate-melt electrolytes for high-energy-density aqueous batteries. *Nat. Energy* **2016**, *1*, 1–9. [CrossRef]
29. Kühnel, R.-S.; Reber, D.; Battaglia, C. A high-voltage aqueous electrolyte for sodium-ion batteries. *ACS Energy Lett.* **2017**, *2*, 2005–2006. [CrossRef]
30. Lee, M.H.; Kim, S.J.; Chang, D.; Kim, J.; Moon, S.; Oh, K.; Park, K.-Y.; Seong, W.M.; Park, H.; Kwon, G. Toward a low-cost high-voltage sodium aqueous rechargeable battery. *Mater. Today* **2019**, *29*, 26–36. [CrossRef]
31. Tang, X.; Zhou, D.; Zhang, B.; Wang, S.; Li, P.; Liu, H.; Guo, X.; Jaumaux, P.; Gao, X.; Fu, Y. A universal strategy towards high–energy aqueous multivalent–ion batteries. *Nat. Commun.* **2021**, *12*, 2857. [CrossRef] [PubMed]
32. Cao, L.; Li, D.; Hu, E.; Xu, J.; Deng, T.; Ma, L.; Wang, Y.; Yang, X.-Q.; Wang, C. Solvation structure design for aqueous Zn metal batteries. *J. Am. Chem. Soc.* **2020**, *142*, 21404–21409. [CrossRef] [PubMed]
33. Geng, Y.; Pan, L.; Peng, Z.; Sun, Z.; Lin, H.; Mao, C.; Wang, L.; Dai, L.; Liu, H.; Pan, K. Electrolyte additive engineering for aqueous Zn ion batteries. *Energy Storage Mater.* **2022**, *51*, 733–755. [CrossRef]
34. Lee, C.; Jeong, S.-K. Modulating the hydration number of calcium ions by varying the electrolyte concentration: Electrochemical performance in a prussian blue electrode/aqueous electrolyte system for calcium-ion batteries. *Electrochim. Acta* **2018**, *265*, 430–436. [CrossRef]
35. Chen, M.; Zhang, J.; Ji, X.; Fu, J.; Feng, G. Progress on predicting the electrochemical stability window of electrolytes. *Curr. Opin. Electrochem.* **2022**, *34*, 101030. [CrossRef]
36. Chen, M.; Feng, G.; Qiao, R. Water-in-salt electrolytes: An interfacial perspective. *Curr. Opin. Colloid Interface Sci.* **2020**, *47*, 99–110. [CrossRef]
37. Bi, S.; Wang, R.; Liu, S.; Yan, J.; Mao, B.; Kornyshev, A.A.; Feng, G. Minimizing the electrosorption of water from humid ionic liquids on electrodes. *Nat. Commun.* **2018**, *9*, 5222. [CrossRef]
38. Chen, M.; Wu, J.; Ye, T.; Ye, J.; Zhao, C.; Bi, S.; Yan, J.; Mao, B.; Feng, G. Adding salt to expand voltage window of humid ionic liquids. *Nat. Commun.* **2020**, *11*, 5809. [CrossRef]
39. Vatamanu, J.; Borodin, O. Ramifications of water-in-salt interfacial structure at charged electrodes for electrolyte electrochemical stability. *J. Phys. Chem. Lett.* **2017**, *8*, 4362–4367. [CrossRef]
40. Lv, T.; Suo, L. Water-in-salt widens the electrochemical stability window: Thermodynamic and kinetic factors. *Curr. Opin. Electrochem.* **2021**, *29*, 100818. [CrossRef]
41. Adil, M.; Ghosh, A.; Mitra, S. Water-in-salt electrolyte-based extended voltage range, safe, and long-cycle-life aqueous calcium-ion cells. *ACS Appl. Mater. Interfaces* **2022**, *14*, 25501–25515. [CrossRef] [PubMed]
42. Suo, L.; Oh, D.; Lin, Y.; Zhuo, Z.; Borodin, O.; Gao, T.; Wang, F.; Kushima, A.; Wang, Z.; Kim, H.-C. How solid-electrolyte interphase forms in aqueous electrolytes. *J. Am. Chem. Soc.* **2017**, *139*, 18670–18680. [CrossRef] [PubMed]
43. Huang, X.; Tang, J.; Luo, B.; Knibbe, R.; Lin, T.; Hu, H.; Rana, M.; Hu, Y.; Zhu, X.; Gu, Q. Sandwich-like ultrathin TiS_2 nanosheets confined within N, S codoped porous carbon as an effective polysulfide promoter in lithium-sulfur batteries. *Adv. Energy Mater.* **2019**, *9*, 1901872. [CrossRef]
44. Starnberg, H. Recent developments in alkali metal intercalation of layered transition metal dichalcogenides. *Mod. Phys. Lett. B* **2000**, *14*, 455–471. [CrossRef]
45. Bezerra, C.d.S.; Valerio, M.E.G. Structural and optical study of CaF_2 nanoparticles produced by a microwave-assisted hydrothermal method. *Phys. B Condens. Matter* **2016**, *501*, 106–112. [CrossRef]
46. Demri, B.; Muster, D. XPS study of some calcium compounds. *J. Mater. Process. Technol.* **1995**, *55*, 311–314. [CrossRef]
47. Al-Mamoori, A.; Lawson, S.; Rownaghi, A.A.; Rezaei, F. Improving adsorptive performance of CaO for high-temperature CO_2 capture through Fe and Ga doping. *Energy Fuels* **2019**, *33*, 1404–1413. [CrossRef]
48. Rudolph, W.W.; Irmer, G. Hydration of the calcium (II) ion in an aqueous solution of common anions (ClO_4^-, Cl^-, Br^-, and NO_3^-). *Dalton Trans.* **2013**, *42*, 3919–3935. [CrossRef]
49. Li, M.; Duan, Z.; Zhang, Z.; Zhang, C.; Weare, J. The structure, dynamics and solvation mechanisms of ions in water from long time molecular dynamics simulations: A case study of $CaCl_2$ (aq) aqueous solutions. *Mol. Phys.* **2008**, *106*, 2685–2697. [CrossRef]
50. Han, C.; Li, H.; Li, Y.; Zhu, J.; Zhi, C. Proton-assisted calcium-ion storage in aromatic organic molecular crystal with coplanar stacked structure. *Nat. Commun.* **2021**, *12*, 2400. [CrossRef]
51. Qin, Z.; Song, Y.; Liu, Y.; Liu, X.X. Aqueous calcium-ion storage in amorphous molybdenum oxide. *Chem. Eng. J.* **2023**, *451*, 138681. [CrossRef]
52. Li, L.; Zhang, G.; Deng, X.; Hao, J.; Zhao, X.; Li, H.; Li, B. A covalent organic framework for high-rate aqueous calcium-ion batteries. *J. Mater. Chem. A* **2022**, *10*, 20827–20836. [CrossRef]